Int. J. Electrochem. Sci., 11 **(2016)** 1568 - 1580

International Journal of ELECTROCHEMICAL SCIENCE
www.electrochemsci.org

Effect of Some Rare Earth Oxides Doping on the Morphology, Crystallite Size, Electrical Conductivity and N_2O Decomposition Activity of CuO Catalyst

Bahaa M. Abu-Zied[1,*], *Salem M. Bawaked*[2], *Samia A. Kosa*[2], *Wilhelm Schwieger*[3]

[1] Center of Excellence for Advanced Materials Research (CEAMR), King Abdulaziz University, P.O. Box 80203, Jeddah 21589, Saudi Arabia
[2] Chemistry Department, Faculty of Science, King Abdulaziz University, P.O. Box 80203, Jeddah 21589, Saudi Arabia
[3] Institut Für Chemische Reaktionstechnik, Friedrich-Alexander-Universita¨t Erlangen-Nu¨rnberg, Egerlandstraße 3, 91058 Erlangen, Germany
[*]E-mail: babuzied@kau.edu.sa, babuzied@yahoo.com

Received: 28 September 2015 / *Accepted:* 19 November 2015 / *Published:* 1 January 2016

The present work presents the results of direct catalytic decomposition of nitrous oxide over CuO and its Pr-, Sm- and Tb-promoted catalysts. These catalysts were prepared by the microwave assisted precipitation method, using oxalic acid as precipitant, and subsequent calcination at 500 °C. X-ray diffraction (XRD) was used for identification of the composition of the dried oxalate precursors and their calcination products. Thermogravimetric analysis (TGA) was used to follow up the thermal stability of the prepared precursors. The obtained catalysts were characterized by Fourier transform infrared spectroscopy (FT-IR), field emission scanning electron microscopy (FESEM), transmission electron microscopy, electrical conductivity and (TEM) H_2 temperature programmed reduction (H_2-TPR). An enhancement effect of the added rare earth elements was observed during N_2O decomposition over the prepared catalysts Assessment of the de-N_2O activity was discussed based on the electrical conductivity as well as the H_2-TPR results.

Keywords: Greenhouse gases, N_2O decomposition, nitrous oxide, CuO catalyst, RE promotedCuO

1. INTRODUCTION

Copper II oxide (CuO) is a *p*-type semiconductor, with a narrow band gap of (Eg=1.2 eV) and exhibits the properties of low-dimensional antiferromagnets [1–3]. CuO has been widely applied for diverse applications such as optical, photovoltaic devices, gas sensing, heterogeneous catalysis and ceramic composites [2,4–7]. To date, various methods have been reported for the preparation of

nanocrystalline CuO in different geometrical morphologies. For instance, Xia eta al. [7] have prepared chain-like hierarchically nanostructured CuO by precipitation-reflux method.

Jiang et al. [8] successfully prepared CuO nanosheets via the template-free hydrothermal method. Bozkurt et al. [9] have used the surfactants-assisted precipitation method to prepared nanocrystalline CuO with different morphologies (plate-, rod-, leaf-, particle-, caterpillar-, and corncoblike and nanowires structures). Their results revealed that the surfactant type (including zwitterionic SB12, cationic CTAB and anionic SDS) as well as its addition order to the synthesis environment also affects the morphology of the CuO structures [9]. Liu et al. [10] demonstrated that by changing the volume of PEG200 and the alkalinity during the preparation of CuO nanostructures would tune its morphology from 1D (nanoseeds, nanoribbons) to 3D (shuttle-like, shrimp-like, and nanoflowers).

Nitrous oxide (N_2O) is known to be a greenhouse gas, that has a global warming potential (GWP) of about 310 times of carbon dioxide (CO_2) [11]. N_2O has a very long atmospheric lifetime

(~120 years). Since the citation of N_2O as the second non-CO_2 greenhouse gas, according to the Kyoto Protocol of the United Nations Convention on Climate Change (December 1997), the studies focusing on its abatement has gained more attention. Industrially, N_2O arise as a co-product from some chemical processes, which includes nitric acid production and the production of large amounts of adipic acid, which is produced from the HNO_3 oxidation of cyclohexanol–cyclohexanone mixtures, for Nylon 6,6 and 6,12 [11]. Direct catalytic decomposition of nitrous oxide to its elements (N_2 and O_2) is considered as one of the potential solutions to minimize the N_2O emissions. Various catalysts exhibited promising activity for this reaction such as metals, mixed oxides, supported oxides, spinels, perovskites, and zeolites based catalysts [12–15].

In this contribution, we report effect of doping with some rare earth (RE) elements (Pr, Sm and Tb) on the morphology and crystallite size of CuO nanorparticles, which were prepared via the microwave assisted method of copper oxalate and subsequent calcination at 500 °C. The decomposition pathways of the three RE/copper oxalate mixtures were followed using thermogravimetric analysis (TGA). It was found that the oxalate precursors dehydrate till 150 □C and decompose at the temperature range of 200-400 ^{0}C. Based on thermal analysis results, Pr, Sm, and Tb doped CuO samples were obtained via the calcination, in static air, at 500 □C for 1h for their oxalate precursors. XRD, FTIR, SEM, TEM and XPS analyses were used to characterize the morphology and crystalline quality RE doped copper oxide samples.

2. EXPERIMENTAL

2.1. Catalysts preparation

Copper nitrate ($Cu(NO_3)_2 \cdot 3H_2O$), praseodymium nitrate ($Pr(NO_3)_3 \cdot 6H_2O$), samarium nitrate ($Sm(NO_3)_3 \cdot 6H_2O$), terbium nitrate ($Tb(NO_3)_3 \cdot 6H_2O$), cetyltrimethylammonium bromide (CTAB) and oxalic acid ($H_2C_2O_4$) are of analytical grade chemicals and were used as received without further purification. Copper oxalate precursor was prepared using the microwave assisted precipitation method

employing oxalic acid as precipitant at microwave power (MWP) of 280 W. It is to be mentioned that the selection of the microwave power of 280 W during the precursor preparation was based on our recent results, which indicated that lower MWP yield material with smaller particles size [16]. CuO was obtained by the subsequent calcination of the copper oxalate precursor for 1 h at 500 °C in air. The three rare earths promoted CuO catalysts were prepared by the co-precipitation method. In such method the amounts of a rare earth cation (Pr^{3+}, Sm^{3+} and Tb^{3+}), required to achieve a rare earth (RE)/Cu ratio of 0.05, were added during the precipitation of oxalate using the same working procedure. After drying of the co-precipitated oxalates precursors, they were calcined for 1 h at 500 °C in air to yield the corresponding earths promoted CuO catalysts.

2.2. Characterization techniques

The structure and composition of the as-prepared oxalate precursors as well as their calcination products powders were investigated at ambient temperature using Thermo-Scientific ARL X'TRA Powder Diffractometer. TGA measurements were carried out at a heating rate of 10 °C min^{-1} in nitrogen flow (40 ml min^{-1}) with a TA instrument apparatus (model TGA-Q500). The weight of the sample taken in each experiment was around 5 mg. FT-IR spectra (4000–400 cm^{-1}) were recorded using Attenuated Total Reflectance (ATR) sampling accessory on the Nicolet iS50 FT-IR spectrometer. The size and morphology of the prepared catalysts were investigated by using field emission scanning electron microscope (FE-SEM) on a JEOL model JSM-7600F microscope and transmission electron microscopy (TEM) using JEOL (model JEM1011) microscopy. The electrical conductivity of the prepared catalysts was measured using a Pyrex glass cell. In each experiment a 0.5 g of the catalyst powder was placed between two silver electrodes having 1.0 cm diameter. The resistance measurements were carried out using Keithley 6517A electrometer. Hydrogen temperature-programmed reduction (H_2-TPR) experiments were performed on Quantachrome CHEMBET-3000 instrument operated with a TCD detector. In each experiment, the catalyst was pre-treated in helium at 300 °C for 30 min followed by cooling to 25 °C. Then, the flow of the gas was changed to 5% H_2+ 95% Ar and the sample temperature increased to 600◦C at the rate of 5 °C/min.

2.3. Activity measurements

The catalytic decomposition of N_2O was performed in a continuous flow quartz-glass reactor, at atmospheric pressure, containing approximately 500 mg of the catalyst. The experiments were carried out at the temperature range between 150 and 500 °C and a W/F value of 0.15 g s cm^{-3}. The N_2O gas was introduced onto the catalyst bed from the bottom. The reactor was heated using a temperature-controlled furnace. The temperature in the reactor was regulated and measured using a thermocouple on the catalyst bed. Prior to the reaction the catalyst was heated to 500 °C in helium flow and kept at that temperature for 1 h. The reactant gas, 500 ppm N_2O, was introduced to the catalyst bed with the aid of Bronkhorst thermal mass flow controllers using helium as a balance gas. The N_2O

concentrations in the inlet and outlet streams were measured using non-dispersive infrared analyzer (Hartmann and Braun, Uras 10E).

3. RESULTS AND DISCUSSION

3.1. Catalysts Characterization

Fig. 1 shows the XRD patterns of the obtained oxalates precursors. The obtained patterns reveal the crystalline nature of the prepared precursors. All the diffraction peaks of the copper oxalate (Fig. 1(a)) match well with those of orthorhombic phase of copper oxalate (JCPDS 21– 0297, space group Pnnm) and are similar to the XRD patterns reported by other research groups [1,4,17–19]. No other peaks, due to the presence of impurities, were identified. This, in turn, suggests the formation of purely crystalline $CuC_2O_4.H_2O$. The diffractograms of the RE-promoted copper oxalate precursors (Fig. 1(b–d)) reveals the presence of the reflections due to copper oxalate together with small reflections at 2θ = 10–20° and 24-29°. These reflections could be assigned to the presence of the RE-oxalates.

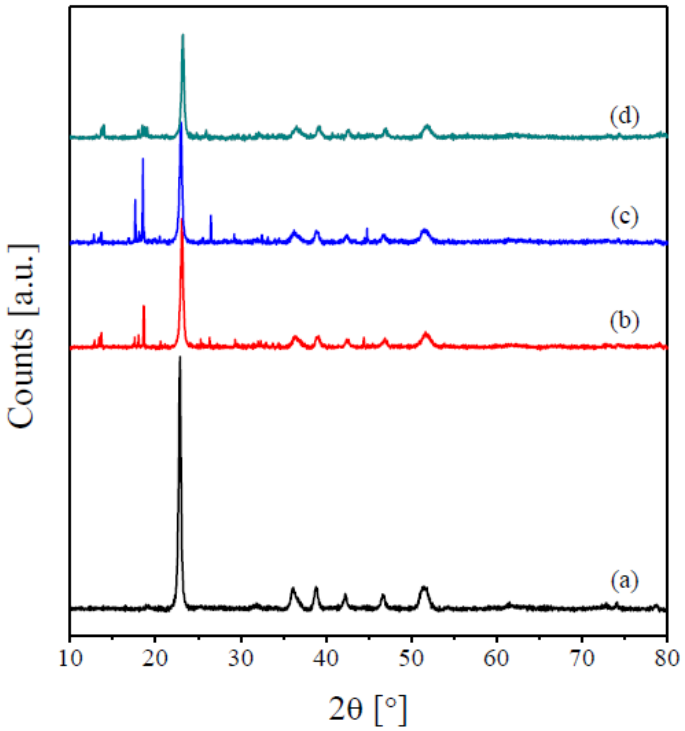

Figure 1. X-ray powder diffraction patterns of Cu oxalate (a), Pr/Cu oxalates (b), Sm/Cu oxalates (c), and Tb/Cu oxalates (d).

Fig. 2 shows the TGA-DTG thermosgrams upon heating the copper oxalate and it RE containing precursors from ambient till 700 °C in nitrogen flow. The thermogram obtained for the copper oxalate (Fig. 2(a)) shows that heating this precursor till 100 °C is accompanied by a small weight loss (WL), which is amounted to around 2 %. This WL could be related to the removal of adsorbed water molecules. Raising the heating temperature resulted in the formation steep WL, which is maximized at 259 °C. The obtained residue in this step (40.9 %) is close to that anticipated to the

formation of Cu_2O (41.3 %). Similar results were reported by Lamprecht et al. for the decomposition of copper oxalate in argon and nitrogen flows [17]. In this context, it was shown that the decomposition of copper oxalate in air flow proceeds with the formation of CuO [19,20].

The obtained TGA-DTG thermograms for the RE-containing precursors (Fig. 2(b–d)) reveal the presence of three WL steps. These steps are maximized at the temperature ranges of 60–89 °C, 268–275 °C and 379–413 °C. By comparison with the TGA-DTG curves of copper oxalate, the obtained curves (Fig. 2(b–d)) could reasonably related to the precursors-dehydration, copper oxalate decomposition and RE-oxalates decomposition, respectively. Based on the TGA-DTA results the various parents were calcined at 500 °C for 1h in order to obtain the relevant CuO as well as the RE-promotes CuO catalysts.

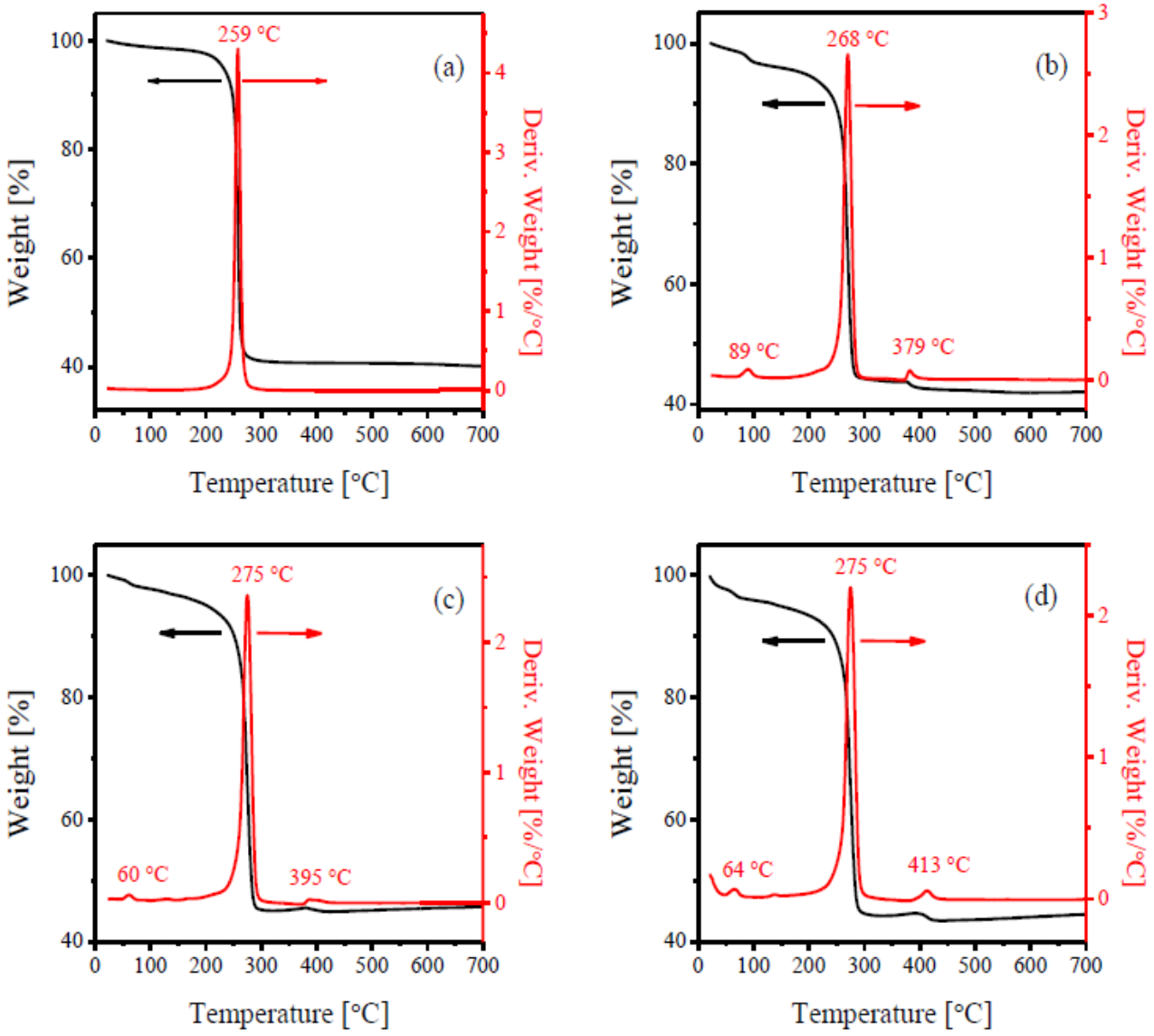

Figure 2. TGA-DTG curves obtained for the Cu-oxalate (a), Pr/Cu-oxalate (b), Sm/Cu-oxalate (c), and Tb/Cu-oxalate (d).

Typical XRD patterns of the calcination products of copper and its RE-containing oxalates are shown in Fig. 3. Fig. 3(a) reveals that calcining the parent copper oxalate at 500 °C is accompanied by a complete disappearance of all reflections due to the oxalate phase and the emergence of new reflections at 2 θ = 32.65°, 35.57°, 38.79°, 46.38°, 48.91°, 53.53°, 58.38°, 61.65°, 65.85°, 66.38°, 68.08°, 72.44°, 75.06° and 75.36°. These reflections agree well with those reported for the monoclinic phase of CuO (JCPDS 80-1917, space group Cc). No peaks due to the presence of impurities were observed in the XRD pattern. This indicates the complete decomposition of copper oxalate in air leading to the formation of pure CuO as the decomposition product. The XRD pattern of the Pr-containing CuO (Fig. 3(b)) reveals the presence of all reflections due to the monoclinic CuO together with very-small intensity ones at 2θ = 28.27°, and 46.432°. These reflections could be assigned to Pr_6O_{11} phase (JCPDS 42-1121), which suggests that this catalyst is composed of CuO as a major phase together with trace amount of Pr_6O_{11}. In addition to the peaks characterizing the monoclinic CuO phase, the diffractogram of the calcined Sm/Cu (Fig. 3(c)) reveals the existence of a weak reflection at 2θ = 28.24°. This reflection could be assigned to the Sm_2O_3 phase (JCPDS 76-0153). This, in turn, suggests the co-existence of CuO (major) and Sm_2O_3 (trace) for this sample. Finally, the composition of the calcined Tb/Cu can be suggested to be CuO (major) and Tb_4O_7 (trace). This can be judged from the existence of all reflections due to monoclinic CuO together with the emergence a new weak reflection at 2θ = 28.31°, which could be due to the presence of Tb_4O_7 (JCPDS card No. 13-0387). The broadening of the XRD peaks of the catalysts presented in Fig. 4 indicates nanometer size of these calcination products. The crystallite sizes of these catalysts were determined from the XRD line broadening applying the Scherrer formula [12,21]. The obtained values are listed in Table 1. The obtained values indicate that doping CuO with the various RE-oxides leads to a noticeable decrease in its crystallite sizes.

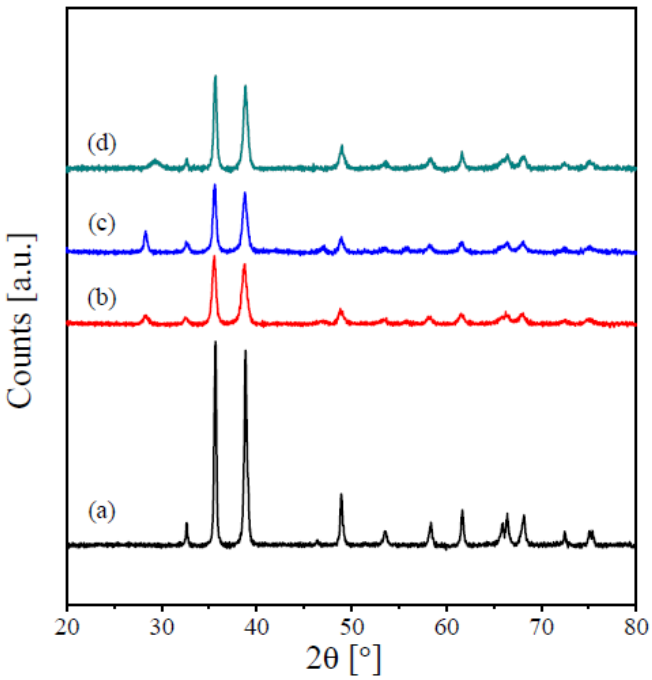

Figure 3. X-ray powder diffraction patterns of CuO (a), Pr/CuO (b), Sm/CuO (c), and Tb/CuO (d) catalysts.

Table 1. Crystallite sizes, electrical conductivities, T_{25} and T_{50} values obtained for bare CuO ant its REpromoted catalysts.

Catalyst	Crystallite size [nm]	$\sigma \times 10^{-5}$ [Ω^{-1} cm^{-1}]	T_{25} [°C]	T_{50} [°C]
CuO	53.5	2.0	446	497
Pr/CuO	15.8	25.9	385	458
Sm/CuO	18.9	46.5	390	451
Tb/CuO	23.7	45.5	408	463

The FT-IR spectra of as prepared CuO and its RE-containing catalysts are shown in Fig. 4. All the spectra revealed the presence of strong absorptions located at 500–600 cm^{-1} assignable CuO vibration in CuO [1,22–24]. The RE oxide containing catalysts reveals the presence of other weak absorptions at the wavenumber range of 1700-1200 cm^{-1}, which can be assigned to the presence of surface carbonate species. This suggests the ability of the added RE oxides to form weak surface carbonates upon contact with atmospheric air [21,25].

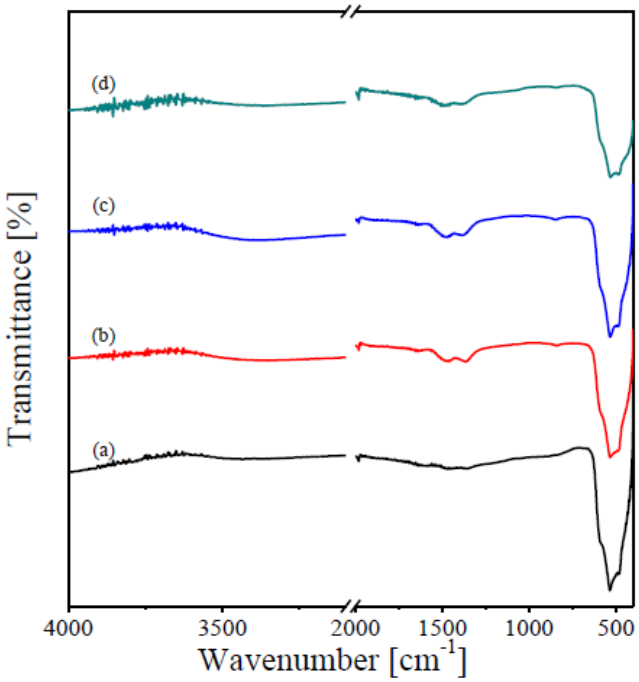

Figure 4. FT-IR spectra taken for CuO (a), Pr/CuO (b), Sm/CuO (c), and Tb/CuO (d) catalysts.

Fig. 5 depicts the high-magnification FE-SEM images of the obtained CuO and its RE doped catalysts. From the obtained nanograph, it was observed that the nanocrystalline CuO (Fig. 5(a)) consists of uniform spheres with an average diameter of about 1-2 μm. These microspheres consist of smaller agglomerates having a sphere-like morphology too with diameters in the range of 50-200 nm. Concurrent to this observation, the work of Behnoudnia and Dehghani [1], who reported the formation

of sphere-like and rice-like morphologies of CuO nanoparticles via the heating of $CuC_2O_4.H_2O$ alone and $CuC_2O_4.H_2O$ and NaOH mixture, respectively. Similar spherelike morphology, with diameters in the range 13.3–31.2 nm, was reported by Jayaprakash et al. [24], for their CuO prepared by the sol–gel method and subsequent annealing at 400 °C. Jia et al. [19] demonstrated that morphology of CuO prepared by the decomposition of $CuC_2O_4.H_2O$ depends also on the copper ions source; sphere-like particles were obtained using $CuSO_4$ and $CuCl_2$ precursors where a biscuit-like morphology was obtained using $Cu(CH_3COO)_2$ precursor. Regarding the effect of the added RE-oxides, our results (Fig. 5(b–d)) indicated that the REoxides/CuO solids maintain the sphere-like morphology of CuO. Moreover the Pr- and Sm containing catalysts are more porous and have smaller agglomerates.

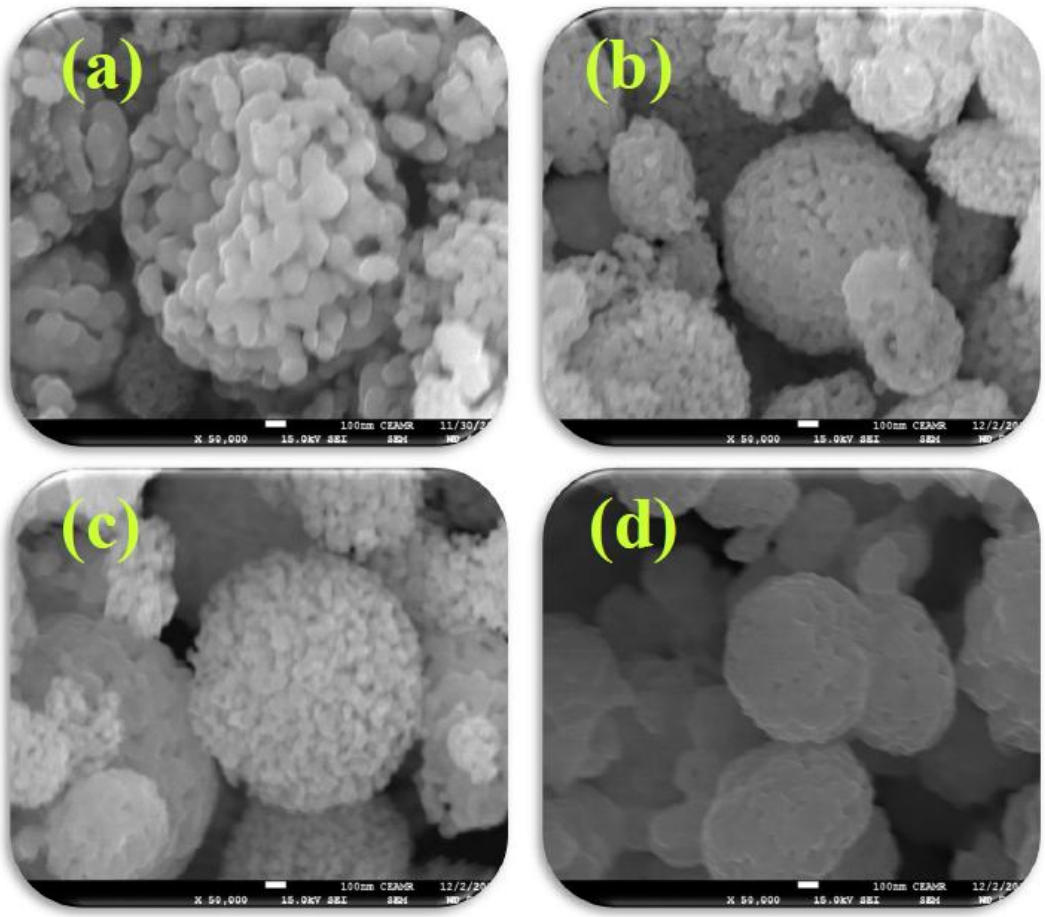

Figure 5. FE-SEM nano-graphs obtained for CuO (a), Pr/CuO (b), Sm/CuO (c), and Tb/CuO (d) catalysts.

The TEM image of the bare CuO (Fig. 6(a)) indicates that it is composed of sets of welded sphere-like particles having diameters in the range 80-160 nm. TEM images of the various RE containing CuO catalysts (Fig. 6(b–d)) exhibit the same sphere-like morphology. However, the particles of such spheres have smaller diameters than those of the bare CuO. The various particles of each oxide mixture are also welded and clear boundaries of the nanomaterials can be observed. The information abstracted form the electron microscopy investigations are in line with those obtained from the XRD analysis.

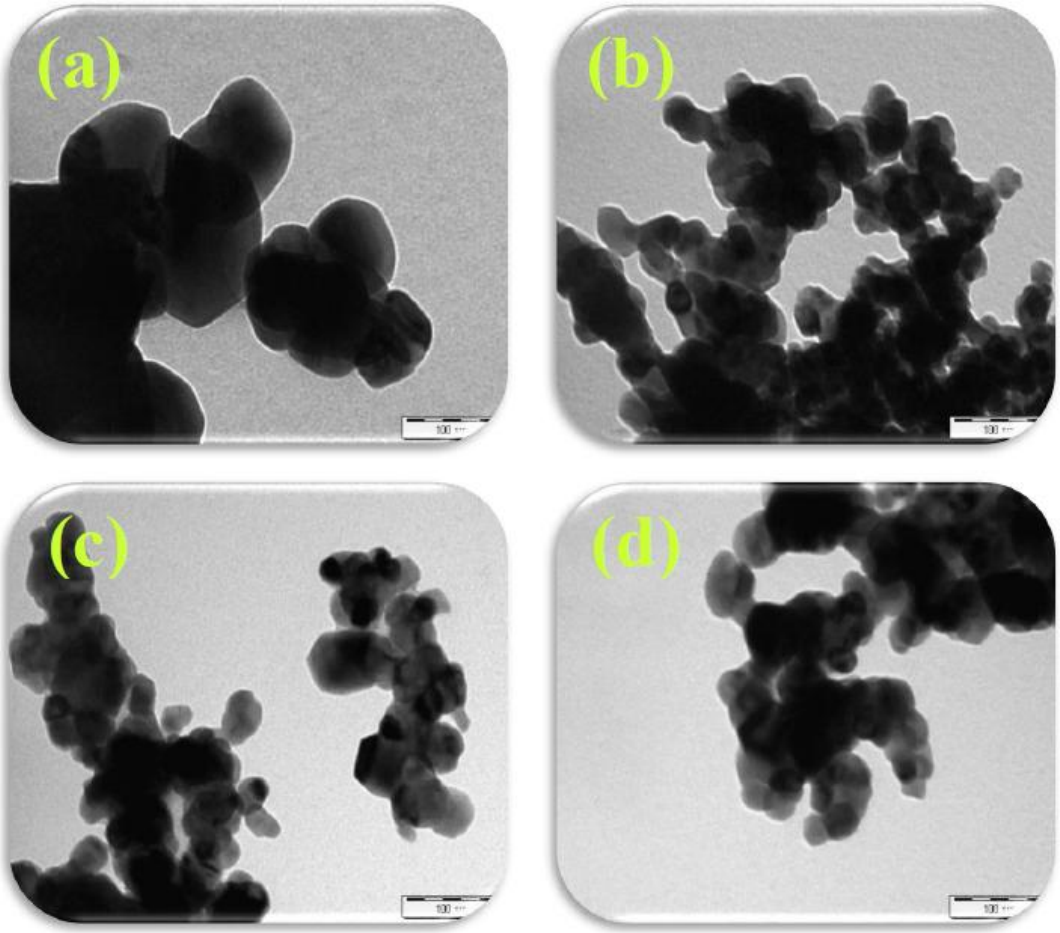

Figure 6. TEM images obtained for CuO (a), Pr/CuO (b), Sm/CuO (c), and Tb/CuO (d) catalysts.

3.2. N_2O decomposition activity

The catalytic activity of the bare CuO and tis RE-promoted catalysts was tested for direct N_2O decomposition and compared with that of the un-promoted CuO. Fig. 7 shows the conversions % of N_2O to N_2 and O_2 obtained over the bare CuO catalyst and its RE-promoted ones in the reactor temperature range 200–500 °C. The CuO catalyst displays a significant N_2O conversion above 300 °C and a reaches a conversion of 51 % at 500 °C. The obtained T_{25} and T_{50} values, which are the temperatures at 25 and 50 N_2O conversion %, respectively, are listed in Table 1. With respect to the activity of the RE-promoted CuO catalysts, Fig. 7 and Table 1 reveal that all the RE-promoted catalysts exhibit higher activity profiles compared to the un-promoted CuO. Meanwhile, the activity increases continuously with the reactor temperature all over the tested catalysts.

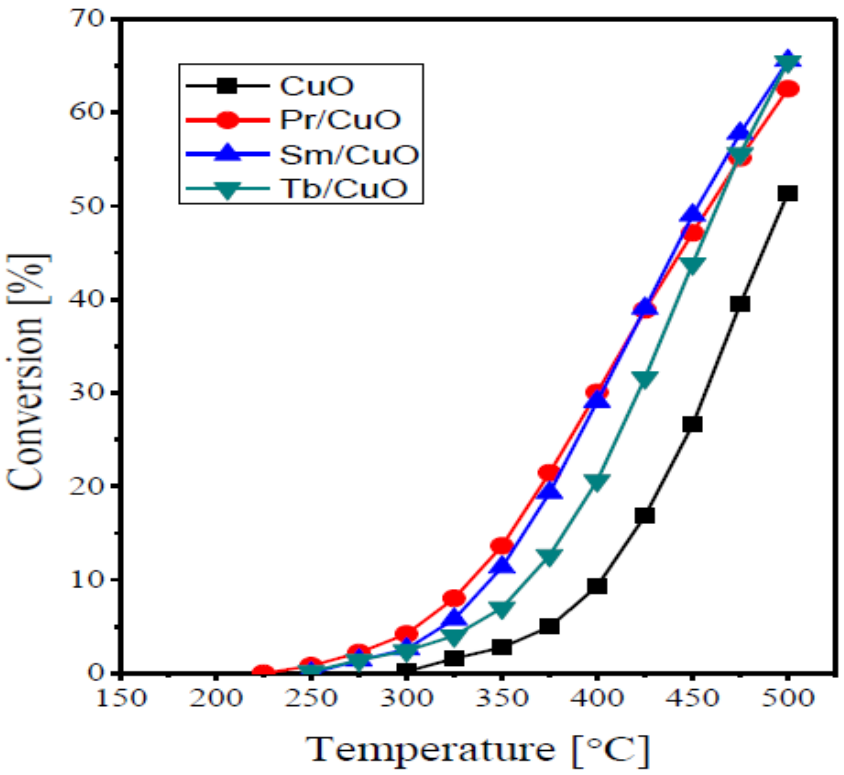

Figure 7. Dependence of N_2O conversion % on the reaction temperature over the CuO, Pr_6O_{11}/CuO, Sm_2O_3/CuO and Tb_4O_7/CuO catalysts.

The promotion effect via doping of various transition-metal based catalysts with different dopants is well documented in the literature. For instant an activity increase was reported for Co_3O_4 based catalysts upon doping with alkali and alkali earth cations [26–28]. An activity promotion was also reported upon doping NiO catalyst with Li, Na, K, and Cs ions during N_2O direct decomposition [29,30]. Regarding N_2O decomposition over CuO catalysts, Pasha et al. [31] reported a superior activity of Cs-promoted catalysts, particularly the molar ratio of Cs/Cu at 0.1, compared to the bare CuO. More recently, better catalytic performance during N_2O decomposition over Ce–Cu mixed oxides, prepared by co-precipitation, compared to the bare CuO or CeO_2 [32].

The earlier work of Dell et al. [33] revealed the correlation of the N_2O decomposition activity of a series of metal oxides with their electrical conductivity. The highest activity was exhibited by the *p*-type semiconductors, intermediate activity was exhibited by insulators whereas the *n*-type oxided showed the lowest activity. Based on the *in situ* electrical conductivity measurements, the N_2O abetment activity of a series of transition metal exchanged ZSM-5 zeolites was classified into two series [15]. The first one includes Fe-, Co-, Cu-, Pd-, La-, Ce- and Ag-ZSM-5 catalysts, which showed higher magnitude of electrical conductivity decrease upon the admission of N_2O. On the other hand, the second group contains Ni-, Mn-, Cd-, Zn-, and Y-ZSM-5 catalysts, which exhibited only a mild conductivity decrease during the N_2O admission. Concurrently, the N_2O decomposition activity of Cu-X zeolite catalysts was correlated with their electrical conductivity properties [34]. The reported mechanism for N_2O direct decomposition over various transition-metal based catalysts involves three steps [15,28,32]:

$$N_2{}^{O}{}_{(g)} + M^{n+} \rightarrow N_2O^{-}{}_{(ads.)} .....M^{n+1} \quad \text{..... (1)}$$

$N_2O^-_{(ads.)}$ ..... M^{n+1} → $N_{2(g)}$ + $O^-_{(ads.)}$ ..... M^{n+1} ..... (2)

$O^-_{(ads.)}$ ..... M^{n+1} → ½$O_{2(g)}$ + M^{n+} ..... (3)

The first step in this mechanism includes an electron donation from the catalyst surface to an N_2O molecule leading to its adsorption, i.e. formation of $N_2O^-_{(ads.)}$, and an increase in oxidation state of the active cations at the catalyst surface. It is believed that the added promoters enhances the electron donation ability of the surface transition metal active centers [13,14,26–32]. This means that the reaction is controlled by the electrical properties of the catalyst, where the ability of the electrons to move from the catalyst bulk to its surface is of great importance in enhancing the N_2O adsorption and, thus, decomposition. The conductivity values of bare CuO and its RE-promoted catalysts are listed in Table 1. From the inspection of the obtained values, it appears that doping the bare CuO with the various RE-oxides is accompanied by a noticeable increase of its conductivity. In other words, the electron movement from the catalyst bulk will become more significant when the CuO is doped with the various RE oxides.

Fig. 8 shows the TPR profiles obtained for bare CuO and its Pr-, Sm- and Tb-containing catalysts. The obtained TPR curves of all the catalysts are very similar, which are characterized by the presence of one broad band. This peak could be assigned to the reduction processes Cu^{2+} to Cu^+ and Cu^+ to Cu^0 according to [32,35]:

$CuO + H_2 \rightarrow Cu_2O + H_2O$ ..... (4)

$Cu_2O + H_2 \rightarrow 2\ Cu + H_2O$ ..... (5)

In this respect, Zhang [35] reported that the sequential reduction of copper oxide ($Cu^{2+} \rightarrow Cu^+ \rightarrow Cu^0$) is difficult to be resolve using the H_2-TPR experiments. Inspection of Fig. 8 reveals that all the added RE-oxides shift the H_2-TPR peak towards lower temperatures. This indicates that the incorporation of the RE-oxides enhanced the reducibility of CuO. This finding is in agreement with the results of Zhang et al. [35], who reported a lowering the CuO H_2-TPR peak a result of CeO_2-ZrO_2 incorporation. Similar findings were reported by Konsolakis et al. [32] for Cu-Ce.

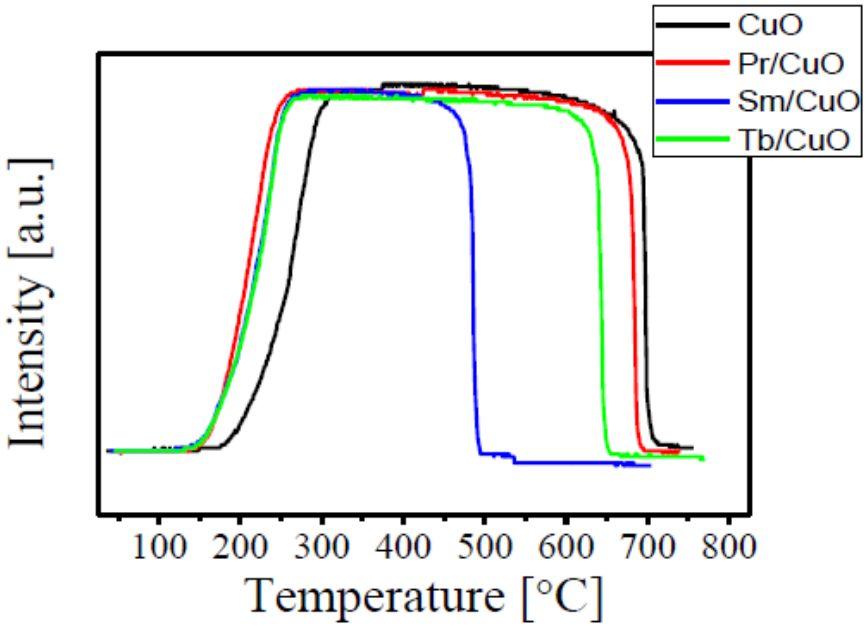

Figure 8. TPR profiles obtained for CuO, Pr/CuO, Sm/CuO, and Tb/CuO catalysts.

It is agreed in the open literature that the added promotors interacts with the active transition metal ions forming an electron-rich species. These species have the electron-donation ability to the adsorbed nitrous oxide molecules, which leads to the weakening of the N-O bond in nitrous oxide and, thus, its decomposition into N_2 molecule and an adsorbed O-species (equations 1 and 2). From the observed increase in the measured electrical conductivity upon incorporating the RE-oxides to CuO, it is plausible to suggest that this will increase the rate of equations 1 and 2 forming Cu^{2+} ions. The recoverability of the copper ions with lower oxidation states, i.e. Cu^{+} ions, is essential for the completion of the reaction mechanism and the regeneration of the active sites. From the observed enhancement of the CuO reducibility (Fig. 8) via RE-oxides addition, we can suggest that these RE-oxides enhance the regeneration of the catalysts active centers, and thus enhancing the N_2O direct decomposition.

4. CONCLUSIONS

In this paper, a series of catalysts comprises of bare CuO and RE-doped CuO was prepared by the microwave assisted precipitation method and subsequent calcination at 500 °C. Structural characterization of the prepared solids indicates that these catalysts are composed of nanocrystalline monoclinic CuO and a mixture of monoclinic CuO together with the RE-oxides, respectively. All the prepared solids showed a sphere-like morphology, where the RE-promoted catalysts exhibit smaller particles size. Higher N_2O decomposition activity RE-promoted catalysts compared to bare CuO. This enhanced activity of the RE-containing catalysts was ascribed to their role in enhancing both the electrical conductance and the reduction of CuO during the catalytic experiments.

ACKNOWLEDGEMENTS
This project was supported by the National Science, Technology and Innovation Plan (MAARIFAH) strategic technologies programs, number (12-ENV2756-03) of the Kingdom of Saudi Arabia. The authors thankfully acknowledge Science and Technology Unit, Deanship of Scientific Research at King Abdulaziz University for their technical support.

References

1. F. Behnoudnia and H. Dehghani, *Polyhedron*, 56 (2013) 102.
2. L. Zhang, R. Liu and H. Yang, *Physica E*, 44 (2012) 1592.
3. A. A. Bush, V. Ya. Shkuratov, A. B. Kuz'menko and E. A. Tishchenko, *Cryst. Rep.*, 47 (2002) 335.
4. X. Zhang, D. Zhang, X. Ni and H. Zheng, *Solid-State Electron.*, 52 (2008) 245.
5. T. Zhang, W. Li and J.-P. Croué, *Appl. Catal. B*, 121–122 (2012) 88.
6. L. Winnubst, P. J. de Veen, S. Ran and D. H. A. Blank, *Ceram. Int.*, 36 (2010) 847.
7. C. Xia, C. Xiaolan, W. Ning and G. Lin, *Anal. Chim. Acta*, 691 (2011) 43.
8. T. Jiang, Y. Wang, D. Meng, X. Wu, J. Wang and J. Chen, *Appl. Surf. Sci.*, 311 (2014) 602.
9. G. Bozkurt, A. Bayrakçeken and A. K. Özer, *Appl. Surf. Sci.*, 318 (2014) 244.

10. J. Liu, J. Jin, Z. Deng, S.-Z. Huang, Z.-Y. Hu, L. Wang, C. Wang, L.-H. Chen, Y. Li, G. Van Tendeloo and B.-L. Su, *J. Colloid Interface Sci.*, 384 (2012) 1.
11. J. Pérez-Ramírez, *Appl. Catal. B*, 70 (2007) 31.
12. B.M. Abu-Zied, *Appl. Catal. A*, 334 (2008) 234.
13. B.M. Abu-Zied, S.A. Soliman and S.E. Abdellah, *J. Ind. Eng. Chem.*, 21 (2015) 814.
14. F. Kapteijn, J. Rodriguez-Mirasol and J. A. Moulijn, *Appl. Catal. B*, 9 (1996) 25.
15. B.M. Abu-Zied, W. Schwieger and A. Unger, *Appl. Catal. B*, 84 (2008) 277.
16. B. M. Abu-Zied, S. M. Bawaked, S. A. Kosa and W. Schwieger, *Appl. Surf. Sci.*, 351 (2015) 600.
17. E. Lamprecht, G. M. Watkins and M. E. Brown, *Thermochim. Acta*, 446 (2006) 91.
18. D. X. Zhang, H. Xu, Y. Z. Liao, H. S. Li and X. J. Yang, *Powder Technol.*, 189 (2009) 404.
19. Z. Jia, L. Yue, Y. Zheng and Z. Xu, *Mater. Res. Bull.*, 43 (2008) 2434.
20. A. Aimable, A. T. Puentes and P. Bowen, *Powder Technol.*, 208 (2011) 467.
21. B.M. Abu-Zied and S.A. Soliman, *Thermochim. Acta*, 470 (2008) 91.
22. A. B. Devi, D. S. Moirangthem, N. C. Talukdar, M. D. Devi, N. R. Singh and M. N. Luwang, *Chin. Chem. Lett.*, 25 (2014) 1615.
23. J. K. Sharma, M. S. Akhtar, S. Ameen, P. Srivastava and G. Singh, *J. Alloys Compd.*, 632 (2015) 321.
24. J. Jayaprakash, N. Srinivasan, P. Chandrasekaran and E. K. Girija, *Spectrochim. Acta, Part A*, 136 (2015) 1803.
25. S.A. Soliman and B.M. Abu-Zied, *Thermochim. Acta*, 491 (2009) 84.
26. G. Maniak, P. Stelmachowski, A. Kotarba, Z. Sojka, V. Rico-Pérez and A. Bueno-López, *Appl. Catal. B*, 136–137 (2013) 302.
27. N. Pasha, N. Lingaiah, N. S. Babu, P. S. S. Reddy and P. S. S. Prasad, *Catal. Commun.*, 10 (2008) 132.
28. B. M. Abu-Zied and S. A. Soliman, *Catal. Lett.*, 132 (2009) 299.
29. N. Pasha, N. Lingaiah, P. S. S. Reddy and P. S. S. Prasad, *Catal. Lett.*, 118 (2007) 64.
30. B.M. Abu-Zied and A.M. Asiri, *Chin. J. Catal.*, 36 (2015), proof (doi: 10.1016/S18722067(15)60963-9).
31. N. Pasha, N. Lingaiah, P. S. S. Reddy and P. S. S. Prasad, *Catal. Lett.*, 127 (2009) 101.
32. M. Konsolakis, S. A. C. Carabineiro, E. Papista, G. E. Marnellos, P. B. Tavares, J. Agostinho Moreira, Y. Romaguera-Barcelay and J. L. Figueiredo, *Catal. Sci. Technol.*, 5 (2015) 3714.
33. R. M. Dell, F. S. Stone and P. F. Tiley, Trans. Faraday Soc. 49 (1953) 201.
34. B. M. Abu-Zied, Microporous Mesoporous Mater., 139 (2011) 59.
35. Q. Zhang, L. Xu, P. Ning, J. Gu and Q. Guan, *Appl. Surf. Sci.*, 317 (2014) 955.